Mobility-Energy Resilience under Blackout Risk via Optimal V2G Management

Fumihito Furuhashi[1], Seigo Yakushijin[1], Soga Shigemura[1], and Eiji Hato[1]

[1]Department of Civil Engineering, The University of Tokyo, Japan

Abstract

This study examines how Vehicle-to-Grid (V2G) can either strengthen or weaken the resilience of electric demand-responsive transport (e-DRT) under blackout risk. We develop a blackout-aware resilient operation framework that evaluates fleet decisions over a 16-hour horizon under blackout uncertainty. Before blackout realization, the operator chooses routing, charging/discharging, reserve state of charge, and vehicle pre-positioning; after the disruption materializes, the fleet adapts to emergency power supply and priority transport under the realized outage conditions. The underlying formulation uses a preparedness-response decomposition with scenario-based post-disruption evaluation. Numerical experiments on a 20-node system with four EVs and four critical facilities report a representative 14:00–18:00 blackout realization, in which a resilience-aware V2G policy outperforms a profit-oriented V2G strategy. Compared with profit-oriented control, the proposed policy increases passenger service from 46.8% to 54.8%, priority-trip fulfillment from 60.0% to 80.0%, and critical-load supply from 38.4% to 42.6%, while also improving blackout-onset fleet SOC and the day-level objective value through faster recovery. The results indicate that V2G supports urban resilience only when reserve energy and vehicle positioning are explicitly coordinated across preparedness and post-disruption response.

Keywords: Blackout uncertainty, Resilient operation, Demand-responsive transport, Electric vehicle, Vehicle-to-Grid

1 Introduction

Recent regional conflict has renewed attention to the Strait of Hormuz as a critical oil chokepoint (U.S. Energy Information Administration, 2025), underscoring the need for mobility-energy systems that remain functional under blackout and fuel-security risk. This study develops a blackout-aware resilient operation framework for V2G-integrated electric demand-responsive transport (e-DRT) under outage uncertainty. Figure 1 summarizes the core mechanism: the same EV fleet serves transport demand in the preparedness period, then shifts to emergency mobility and direct power support after blackout onset, so pre-outage charging, routing, and vehicle positioning determine post-disruption capability.

This study focuses on low-density areas, where DRT is increasingly used to maintain accessibility when fixed-route transit is difficult to sustain (Vansteenwegen et al., 2022; Lu et al., 2023). Electrification improves the long-run feasibility of these services, but it also makes the battery both a mobility constraint and a distributed energy resource, motivating recent work on V2G and integrated mobility-energy operation (Kempton & Tomić, 2005a,b; Ma & Fang, 2022).

Most e-DRT and electric dial-a-ride studies optimize routing and charging to preserve service feasibility or reduce operating cost (Bongiovanni et al., 2019; Ma, 2021; Li et al., 2022; Lian et al., 2023). Shared-mobility V2G studies likewise emphasize price arbitrage under known electricity-price trajectories (Iacobucci et al., 2018, 2019; Liao et al., 2021; Zeng et al., 2023; He et al., 2025), leaving the disrupted-power context largely unaddressed. This omission matters for urban resilience. If an operator discharges EV batteries before a possible outage to exploit a temporary price spike, the fleet may lose the ability to

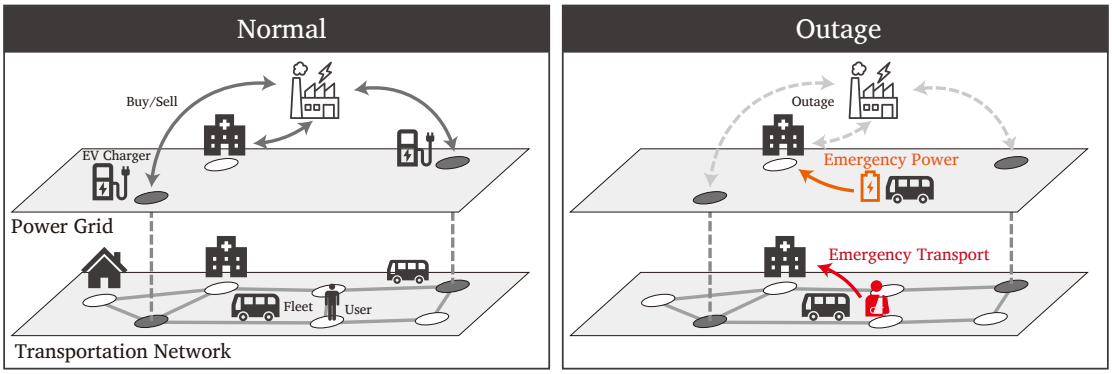


Figure 1: Conceptual illustration of blackout-aware V2G-integrated e-DRT operation under blackout uncertainty. The left panel shows the pre-disruption preparedness period, in which the fleet serves users on the transportation network while buying electricity from and selling electricity to the grid through EV chargers. The right panel shows the post-disruption response period, in which grid exchange is disrupted and the same fleet is repurposed to provide emergency power and emergency transport. The contrast emphasizes that pre-outage routing, charging, and pre-positioning decisions determine how much mobility and backup energy service can be sustained after blackout onset.

support hospitals, shelters, or telecommunications facilities when blackout occurs. The design problem is therefore not only how to earn V2G revenue in normal times, but how to balance revenue, mobility service, and emergency functionality under outage risk.

We treat EVs as dual-purpose assets that can transport passengers during normal operation and serve as portable power sources when outages occur. The operating day is partitioned at a contingency decision boundary $t^c = 14{:}00$. Before that boundary, the operator chooses routing, charging, reserve-SOC, and vehicle pre-positioning decisions without knowing when or in what form a blackout contingency may materialize within the modeled uncertainty set. Once a blackout occurs, the fleet is reallocated through contingency-specific post-disruption response to support priority mobility and emergency power service under the realized disruption. For numerical exposition in Section 4, we instantiate the general formulation on a representative singleton blackout realization $\omega^\star$ with unit probability, in which the blackout window spans 14:00–18:00. This framework explicitly evaluates how reserve state of charge, vehicle pre-positioning, and grid unavailability shape functional continuity after disruption.

The contributions are threefold. First, we extend the conventional routing-and-charging formulation by introducing blackout uncertainty, critical facilities, reserve-SOC targets, and unmet critical-load penalties. Second, we model how preparedness decisions before blackout realization determine mobility and emergency-power performance under the realized disruption. Third, we show numerically that the resilience-aware policy improves performance relative to a profit-oriented V2G policy on a representative blackout realization, thereby exposing the paradox that V2G can either enhance or undermine resilience depending on how energy reserves are managed.

2 Methodology

System setting

We consider an electric DRT fleet operating on a spatial network $(\mathcal{N}, \mathcal{A})$ over the service period from 6:00 to 22:00. Time is discretized into 5-minute steps. The vehicle set is denoted by $\mathcal{K}$, the pre-disruption regular passenger-demand set by $\mathcal{R}^{\text{pre}}$, and the subset

of charging-capable nodes by $\mathcal{N}^{\mathrm{chg}} \subseteq \mathcal{N}$.

To model blackout resilience under uncertainty, we split the day at a contingency decision boundary t^c = 14:00. The pre-disruption stage $\mathcal{T}^{\mathrm{pre}}$ spans 6:00–14:00 and the post-disruption stage $\mathcal{T}^{\mathrm{post}}$ spans 14:00–22:00. At t^c, one disruption pattern $\omega \in \Omega$ may materialize from a finite outage set with probabilities p_ω. Each scenario specifies a blackout-response window $\mathcal{T}^{\mathrm{blk}}_\omega \subseteq \mathcal{T}^{\mathrm{post}}$, a blackout-affected facility set $\mathcal{N}^{\mathrm{blk}}_\omega \subseteq \mathcal{N}^{\mathrm{crit}}$, scenario-specific emergency loads $D^{\mathrm{crit}}_{i,t,\omega}$, scenario-specific post-disruption regular requests $\mathcal{R}^{\mathrm{reg}}_\omega$, and scenario-specific priority requests $\mathcal{R}^{\mathrm{pri}}_\omega$. Preparedness decisions must be chosen before the realized disruption is known. In the numerical section, the finite-scenario formulation is instantiated on a singleton benchmark $\Omega = \{\omega^\star\}$ with $p_{\omega^\star} = 1$, where the blackout spans 14:00–18:00 and affects all four critical facilities.

We further define a set of critical facilities $\mathcal{N}^{\mathrm{crit}} \subseteq \mathcal{N}$, consisting of one hospital, two shelters, and one telecommunications node. During the blackout-response window of scenario ω, each affected facility $i \in \mathcal{N}^{\mathrm{blk}}_\omega$ requires an emergency load $D^{\mathrm{crit}}_{i,t,\omega}$ [kWh]. In addition to the pre-disruption regular requests $\mathcal{R}^{\mathrm{pre}}$, each scenario contains a set of post-disruption regular requests $\mathcal{R}^{\mathrm{reg}}_\omega$ and a set of priority requests $\mathcal{R}^{\mathrm{pri}}_\omega$. The former represent regular passenger service that resumes after blackout onset and grid recovery, whereas the latter represent evacuation and medical-access trips.

Before t^c, vehicles may charge from or discharge to the grid at nodes in $\mathcal{N}^{\mathrm{chg}}$. During the blackout-response window, grid transactions are suspended at all charging nodes, and EVs can discharge only by directly supplying electricity to critical facilities when physically present at those nodes. Consequently, stored energy has two different values over the day: arbitrage value before 14:00 and resilience value after 14:00.

Preparedness-response formulation under blackout uncertainty

We represent one operating day through a preparedness-response formulation under blackout uncertainty. The pre-disruption layer consists of regular passenger assignment, routing, charging/discharging, and pre-positioning decisions executed over $\mathcal{T}^{\mathrm{pre}}$ before the blackout outcome is known. The post-disruption layer consists of contingency-specific reallocation, post-disruption regular passenger service, priority passenger service, and emergency supply to critical facilities once a blackout occurs. The day-level objective is

$$
\begin{aligned}
\max \quad & \sum_{r \in \mathcal{R}^{\mathrm{pre}}} F_r z_r + \sum_{k \in \mathcal{K}} \sum_{t \in \mathcal{T}^{\mathrm{pre}}} \left(p^{\mathrm{sell}}_t v^{\mathrm{dis}}_{k,t} - p^{\mathrm{buy}}_t v^{\mathrm{ch}}_{k,t} \right) \\
& - \alpha \sum_{r \in \mathcal{R}^{\mathrm{pre}}} \left(\delta^{\mathrm{p}}_r + \delta^{\mathrm{d}}_r \right) - \beta \sum_{r \in \mathcal{R}^{\mathrm{pre}}} u^{\mathrm{miss}}_r - \rho \sum_{k \in \mathcal{K}} \xi_k \\
& + \sum_{\omega \in \Omega} p_\omega \Bigg[\sum_{r \in \mathcal{R}^{\mathrm{reg}}_\omega} F_r z^{\mathrm{reg}}_{r,\omega} - \beta \sum_{r \in \mathcal{R}^{\mathrm{reg}}_\omega} u^{\mathrm{reg,miss}}_{r,\omega} \\
& \quad + \sum_{r \in \mathcal{R}^{\mathrm{pri}}_\omega} F_r z^{\mathrm{pri}}_{r,\omega} - \beta \sum_{r \in \mathcal{R}^{\mathrm{pri}}_\omega} u^{\mathrm{pri,miss}}_{r,\omega} - \gamma \sum_{i \in \mathcal{N}^{\mathrm{blk}}_\omega} \sum_{t \in \mathcal{T}^{\mathrm{blk}}_\omega} s_{i,t,\omega} \Bigg].
\end{aligned} \tag{1}
$$

Here, z_r indicates whether pre-disruption regular request r is served in the preparedness layer. The variable u^{miss}_r denotes unmet regular demand; when unmet demand is modeled in binary form, it is linked to service acceptance by $u^{\mathrm{miss}}_r = 1 - z_r$. The terms δ^p_r and δ^d_r denote the pickup and drop-off delay for request r, respectively. Moreover, $z^{\mathrm{reg}}_{r,\omega}$ and $z^{\mathrm{pri}}_{r,\omega}$ denote the served fractions of post-disruption regular and priority request r in scenario ω, respectively, while $u^{\mathrm{reg,miss}}_{r,\omega}$ and $u^{\mathrm{pri,miss}}_{r,\omega}$ denote the corresponding unmet-demand fractions. The variable $s_{i,t,\omega}$ is the unmet critical-load slack at facility i and time t in scenario ω, and ξ_k represents the shortfall from the minimum reserve SOC required at the contingency boundary. To preserve the validity of the dual-based decomposition in Section 3, the post-

disruption recourse layer is evaluated through an LP relaxation:

$$z^{\mathrm{reg}}_{r,\omega},\ z^{\mathrm{pri}}_{r,\omega},\ u^{\mathrm{reg,miss}}_{r,\omega},\ u^{\mathrm{pri,miss}}_{r,\omega},\ x^{\mathrm{post}}_{k,t,i,\omega} \in [0,1]. \tag{2}$$

They should therefore be interpreted as service and location intensities in the recourse approximation rather than binary dispatch commitments. The coefficients α, β, γ, and ρ govern the trade-off among transport performance, pre-disruption profit, and expected emergency capability.

The emergency supply decision is represented by $v^{\mathrm{sup}}_{k,t,i,\omega} \geq 0$, i.e., the electricity delivered by vehicle k to critical node i at time t in scenario ω. Critical-load satisfaction is written as

$$\sum_{k\in\mathcal{K}} v^{\mathrm{sup}}_{k,t,i,\omega} + s_{i,t,\omega} \geq D^{\mathrm{crit}}_{i,t,\omega} \qquad (\forall \omega \in \Omega,\ \forall i \in \mathcal{N}^{\mathrm{blk}}_{\omega},\ \forall t \in \mathcal{T}^{\mathrm{blk}}_{\omega}). \tag{3}$$

Emergency supply is feasible only when the vehicle is located at the corresponding critical node:

$$0 \leq v^{\mathrm{sup}}_{k,t,i,\omega} \leq M x^{\mathrm{post}}_{k,t,i,\omega} \qquad (\forall \omega \in \Omega,\ \forall k \in \mathcal{K},\ \forall i \in \mathcal{N}^{\mathrm{blk}}_{\omega},\ \forall t \in \mathcal{T}^{\mathrm{blk}}_{\omega}), \tag{4}$$

where $x^{\mathrm{post}}_{k,t,i,\omega} \in [0,1]$ is the LP-relaxed post-disruption presence intensity of vehicle k at node i and time t in scenario ω.

Grid transactions are disabled during the blackout-response window:

$$v^{\mathrm{ch}}_{k,t,\omega} = v^{\mathrm{dis}}_{k,t,\omega} = 0 \qquad (\forall \omega \in \Omega,\ \forall k \in \mathcal{K},\ \forall t \in \mathcal{T}^{\mathrm{blk}}_{\omega}). \tag{5}$$

Battery dynamics in scenario ω follow

$$c^{\mathrm{post}}_{k,t+1,\omega} = c^{\mathrm{post}}_{k,t,\omega} + \eta^{\mathrm{ch}}_{k} v^{\mathrm{ch}}_{k,t,\omega} - \frac{v^{\mathrm{dis}}_{k,t,\omega} + \sum_{i\in\mathcal{N}^{\mathrm{blk}}_{\omega}} v^{\mathrm{sup}}_{k,t,i,\omega}}{\eta^{\mathrm{dis}}_{k}} - g_{k,t,\omega}, \tag{6}$$

subject to $\underline{c}_k \leq c^{\mathrm{post}}_{k,t,\omega} \leq \overline{c}_k$. To preserve emergency capability, each vehicle must retain at least c^{res}_{k} kWh at the contingency boundary. The soft reserve constraint is

$$\xi_k \geq c^{\mathrm{res}}_{k} - c^{\mathrm{pre}}_{k,t^c}, \qquad \xi_k \geq 0 \qquad (\forall k \in \mathcal{K}), \tag{7}$$

so the model may violate the reserve target only by paying a penalty.

3 Benders Decomposition for the Preparedness-Response Model

Compact preparedness-response form

This section presents a computational decomposition of the preparedness-response model. It should not be interpreted as assuming that the operator knows the outage in advance; rather, it separates pre-disruption decisions from contingency-specific evaluation after a disruption materializes.

Let $\mathbf{x}$ collect all pre-disruption preparedness decisions over $\mathcal{T}^{\mathrm{pre}}$. These decisions include regular-passenger acceptance, route selection, waiting, pre-disruption charging/discharging, and reserve-positioning decisions. After a blackout contingency $\omega \in \Omega$ materializes at the contingency boundary t^c, the model solves a contingency-specific recourse LP. This recourse problem is the LP relaxation of the post-disruption dispatch layer introduced in Section 2: the service-allocation variables $z^{\mathrm{reg}}_{r,\omega}$ and $z^{\mathrm{pri}}_{r,\omega}$, the unmet-demand variables $u^{\mathrm{reg,miss}}_{r,\omega}$ and $u^{\mathrm{pri,miss}}_{r,\omega}$, and the location variables $x^{\mathrm{post}}_{k,t,i,\omega}$ are continuous on $[0,1]$ when cuts are generated. The overall preparedness-response model can be written in compact form as

$$\max_{\mathbf{x}\in\mathcal{X}^{\mathrm{pre}}} \quad f^{\mathrm{pre}}(\mathbf{x}) + \sum_{\omega\in\Omega} p_\omega Q_\omega(\mathbf{x}), \tag{8}$$

where $f^{\text{pre}}(\mathbf{x})$ denotes the pre-disruption contribution of (1). For a fixed $\mathbf{x}$, the recourse value under contingency ω is

$$\begin{aligned} Q_\omega(\mathbf{x}) = \max_{\mathbf{w}_\omega} \quad & q_\omega^\top \mathbf{w}_\omega \\ \text{s.t.} \quad & A_\omega \mathbf{w}_\omega \le b_\omega - B_\omega \mathbf{x}, \\ & \mathbf{w}_\omega \ge 0. \end{aligned} \tag{9}$$

The vector $\mathbf{w}_\omega$ collects contingency-specific continuous emergency-supply, post-disruption vehicle-state, regular-service, priority-service, and slack variables. The matrix B_ω maps the pre-disruption route, vehicle positions, and SOC at t^c into the contingency-specific initial conditions and resource limits. Importantly, the discrete regular-passenger routing and assignment decisions remain in $\mathbf{x}$; once $\mathbf{x}$ is fixed, each scenario subproblem is linear. Because (9) is an LP, its dual representation is

$$Q_\omega(\mathbf{x}) = \min_{\pi_\omega \in \Pi_\omega} \pi_\omega^\top (b_\omega - B_\omega \mathbf{x}), \qquad \Pi_\omega = \left\{ \pi_\omega \ge 0 : A_\omega^\top \pi_\omega \ge q_\omega \right\}. \tag{10}$$

Equation (10) makes clear that the value of preparedness is transmitted to recourse through the pre-disruption state embedded in $B_\omega \mathbf{x}$.

Master problem and Benders cuts

Introduce one auxiliary variable θ_ω for each scenario to approximate $Q_\omega(\mathbf{x})$. At iteration m, the restricted master problem is

$$\begin{aligned} \max_{\mathbf{x}, \boldsymbol{\theta}} \quad & f^{\text{pre}}(\mathbf{x}) + \sum_{\omega \in \Omega} p_\omega \theta_\omega \\ \text{s.t.} \quad & \mathbf{x} \in \mathcal{X}^{\text{pre}}, \\ & \theta_\omega \le \alpha_\omega^\ell + \left(\beta_\omega^\ell\right)^\top \mathbf{x} \qquad (\forall \omega \in \Omega,\ \forall \ell \in \mathcal{O}_{\omega,m}), \\ & 0 \le \bar{\alpha}_\omega^n + \left(\bar{\beta}_\omega^n\right)^\top \mathbf{x} \qquad (\forall \omega \in \Omega,\ \forall n \in \mathcal{F}_{\omega,m}). \end{aligned} \tag{11}$$

The set $\mathcal{O}_{\omega,m}$ contains optimality cuts for scenario ω, and $\mathcal{F}_{\omega,m}$ contains feasibility cuts generated from dual extreme rays when the scenario subproblem is infeasible.
For a candidate preparedness plan $\mathbf{x}^m$, an optimal dual solution π_ω^m of (10) yields the cut

$$\theta_\omega \le (\pi_\omega^m)^\top (b_\omega - B_\omega \mathbf{x}) \qquad (\forall \omega \in \Omega), \tag{12}$$

which is equivalent to the affine upper bound stored in (11). If the contingency-ω recourse problem is infeasible, a dual ray r_ω^m generates the feasibility cut

$$0 \le (r_\omega^m)^\top (b_\omega - B_\omega \mathbf{x}) \qquad (\forall \omega \in \Omega). \tag{13}$$

Equations (12) and (13) show directly what the decomposition prices: the scenario-weighted marginal value of reserve, charging posture, and pre-positioning before the disruption is known.

Benders solution process

The overall solution process is summarized in Algorithm 1. We use a multi-cut Benders scheme: at each iteration, the master problem proposes a candidate preparedness plan, every scenario subproblem (9) is solved independently, and one cut per violated contingency is added. Because $\mathbf{x}$ contains routing binaries, the master is a MIP, so the procedure can also be interpreted as a branch-and-Benders-cut scheme.

Algorithm 1 Multi-cut Benders decomposition for blackout-aware resilient planning

Initialize lower bound, upper bound, and cut sets $\mathcal{O}_\omega = \emptyset$, $\mathcal{F}_\omega = \emptyset$ for all $\omega \in \Omega$
while termination gap is above tolerance **do**
    Solve the restricted master problem (11)
    Extract the candidate preparedness plan $\mathbf{x}^m$
    for each scenario $\omega \in \Omega$ **do**
        Solve the scenario subproblem $Q_\omega(\mathbf{x}^m)$ in (9)
    end for
    if any scenario subproblem is infeasible **then**
        Generate feasibility cuts of the form (13) for the infeasible scenarios and add them to $\mathcal{F}_\omega$
    else
        Update the incumbent bounds using $f^{\text{pre}}(\mathbf{x}^m) + \sum_{\omega\in\Omega} p_\omega Q_\omega(\mathbf{x}^m)$
        Generate optimality cuts of the form (12) for all scenarios and add them to $\mathcal{O}_\omega$
    end if
end while
Return the preparedness plan and the contingency-specific recourse policies

4 Numerical Experiments

Experimental settings

The proposed framework is evaluated on a stylized 20-node network with four charging/discharging nodes and four EVs. The operating horizon is 6:00–22:00, and time is discretized into 5-minute intervals. The resilience-aware policy is obtained from the preparedness-response model introduced in Sections 2 and 3. For numerical exposition, the finite-scenario formulation is instantiated on a singleton benchmark $\Omega = \{\omega^\star\}$ with probability $p_{\omega^\star} = 1$. In the general model, the uncertain elements are the blackout window, the affected critical facilities, the emergency-load trajectory $D^{\text{crit}}_{i,t,\omega}$, the post-disruption regular requests $\mathcal{R}^{\text{reg}}_\omega$, and the priority requests $\mathcal{R}^{\text{pri}}_\omega$. For the reported representative blackout realization $\omega^\star$, a blackout starts at 14:00 and lasts until 18:00, affecting all four critical facilities simultaneously. This realized event is used for the tables and figures below; the operator is not assumed to know the exact outage onset when making pre-outage routing and charging decisions.

Each vehicle has a 50 kWh battery, an initial SOC of 35 kWh, a charging/discharging limit of 7 kW, and a reserve-SOC target of 20 kWh at blackout onset. Over the day, 40 regular passenger requests are generated; the requests realized before 14:00 belong to $\mathcal{R}^{\text{pre}}$, whereas the regular trips evaluated after the contingency boundary are counted in $\mathcal{R}^{\text{reg}}_{\omega^\star}$. After the blackout begins, 10 additional emergency requests appear in $\omega^\star$, including five priority trips to hospitals or shelters. The outage affects four critical facilities—one hospital, two shelters, and one telecommunications node—with hourly emergency loads of 20, 8, 8, and 5 kWh/h, respectively.

Electricity prices follow a volatile time-of-use profile with a pronounced selling-price spike during 13:00–14:00. This setting creates a direct conflict between pre-outage arbitrage and post-outage preparedness, because discharging before 14:00 can increase short-run revenue while weakening blackout-response capability if the outage materializes. Because $|\Omega| = 1$ in the reported benchmark, the results below should be read as representative realized-event outcomes rather than probability-weighted averages across multiple blackout realizations. The monetary parameters in (1) are set to $\alpha = 10$ JPY/min, $\beta = 3000$ JPY/request, $\gamma = 5000$ JPY/kWh, and $\rho = 2000$ JPY/kWh. The term F_r denotes fare revenue: for regular requests, $F_r = q_r \times 500$ JPY, while priority requests are valued at 1800 JPY for hospital trips and 1200 JPY for shelter trips. All reported day-level objective values are therefore evaluated on a common monetary scale. The preparedness master MIP and

contingency LPs were solved with Gurobi on an Apple M3 Mac, and the Benders procedure was terminated at a relative optimality gap of 1%.

Table 1: Baseline blackout settings

Setting	Value
Spatial nodes	20
Charging/discharging nodes	4
Vehicles	4
Daily passenger requests	40
Scenario count	1
Scenario probability	$p_{\omega^\star} = 1$
Critical facilities	4 (hospital, 2 shelters, telecom)
Time step	5 min
Outage start	14:00
Blackout window	14:00–18:00
Battery capacity	50 kWh
Initial SOC	35 kWh
Reserve SOC target	20 kWh
Emergency requests after blackout	10
Priority emergency requests	5

Case comparison

We compare three cases:

- **Case 1 (Blackout, No V2G):** the representative blackout realization is imposed, but emergency power support through V2G is disabled.
- **Case 2 (Blackout, profit V2G):** V2G is enabled under a profit-oriented control logic.
- **Case 3 (Blackout, resilient V2G):** the proposed resilience-aware V2G policy explicitly values reserve SOC and blackout-onset vehicle positioning.

The three cases differ in how the operating policy is generated. Case 1 disables direct emergency supply by imposing $v^{\mathrm{sup}}_{k,t,i,\omega} = 0$ for all k, i, t, ω. Case 2 retains V2G capability but applies a profit-oriented control logic without resilience-aware reserve protection, whereas Case 3 activates the full resilience-aware control with reserve-SOC protection and pre-positioning incentives. Unless otherwise noted, all metrics in Table 2, including the day-level objective, are evaluated ex post under the common accounting criterion in (1), so the reported values are directly comparable across cases.

Table 2: Results of case comparison. ↑ indicates that higher values are better, and ↓ indicates that lower values are better.

Case	Day-level objective ↑[JPY]	Service ↑[%]	Crit. sup. ↑[%]	Priority ↑[%]	Reserve SOC ↑[kWh]	Unserved ↓[kWh]
C1: Blackout, No V2G	43,209.0	74.2	0.0	60.0	34.11	164.00
C2: Blackout, profit V2G	28,450.8	46.8	38.4	60.0	28.43	101.10
C3: Blackout, resilient V2G	30,761.5	54.8	42.6	80.0	30.56	94.14

Table 2 reports six indicators: day-level objective value, passenger-service ratio, critical-load supply ratio, priority-trip fulfillment ratio, average fleet SOC at blackout onset, and blackout-period unserved critical load. Figure 2 complements these metrics with vehicle schedules, fleet SOC trajectories, and the electricity-price profile. Because only Cases 2 and 3 allow V2G-based emergency support, the core policy comparison is between them, while Case 1 serves as a mobility-only benchmark. The passenger-service ratio is defined as the share of all passenger requests served in the representative blackout realization, with

denominator $|\mathcal{R}^{\mathrm{pre}}| + |\mathcal{R}^{\mathrm{reg}}_{\omega^\star}| + |\mathcal{R}^{\mathrm{pri}}_{\omega^\star}|$. It therefore counts pre-disruption regular service, post-disruption regular service after recovery, and priority trips together, whereas the priority-trip fulfillment ratio isolates only $\mathcal{R}^{\mathrm{pri}}_{\omega^\star}$.

Case 1 highlights the limitation of operating the fleet only for mobility. It achieves the highest day-level objective value (43,209.0 JPY) and passenger-service ratio (74.2%), but because direct emergency support is disabled, it supplies none of the critical load and leaves all 164.00 kWh of blackout-period demand unmet. High transport performance alone therefore does not indicate blackout resilience.

Case 2 shows that enabling V2G alone does not guarantee resilient operation. Under profit-oriented control, the fleet has an incentive to discharge during the 13:00–14:00 price spike, which lowers average fleet SOC at blackout onset to 28.43 kWh. The fleet can then supply 38.4% of critical load, reducing unmet demand to 101.10 kWh, but mobility performance deteriorates: passenger service falls to 46.8%, priority-trip fulfillment remains at 60.0%, and the day-level objective declines to 28,450.8 JPY. V2G thus creates emergency capability, but an arbitrage-oriented policy can still weaken the inherited state at blackout onset.

Case 3 demonstrates the effect of explicitly managing reserve energy and vehicle positioning before the blackout. Relative to Case 2, it enters the outage with a higher average fleet SOC (30.56 versus 28.43 kWh), which raises passenger service to 54.8%, priority-trip fulfillment to 80.0%, and critical-load supply to 42.6%, while reducing unmet critical load to 94.14 kWh and increasing the day-level objective to 30,761.5 JPY. Although Case 3 still serves fewer passengers than the mobility-only benchmark in Case 1, the relevant design comparison is between Cases 2 and 3, and the resilience-aware strategy dominates the profit-oriented V2G strategy on both blackout-service and day-level measures.

Figure 2 clarifies the mechanism behind these aggregate results. Before 14:00, Case 3 allocates more time to charging and less to grid discharge than Case 2, thereby preserving a larger energy buffer. During the blackout window, both V2G-enabled cases redirect vehicles toward direct supply to critical facilities, but Case 3 can sustain more priority transport because it starts the outage with more usable charge and a more favorable vehicle distribution. After grid recovery at 18:00, Case 3 returns more quickly to a mixed pattern of charging and passenger service, whereas Case 2 remains operationally thinner for longer. The figure therefore shows that blackout performance is determined not only by post-outage recourse, but also by the pre-outage charging/discharging pattern that shapes the state inherited from the preparedness period.

Overall, the numerical results support two conclusions. First, V2G should not be evaluated only through short-run market revenue, because aggressive pre-outage discharge can erode emergency capability. Second, the proposed resilience-aware policy improves performance mainly by changing the blackout-onset state of the fleet, thereby improving critical-load coverage, priority mobility, and post-outage recovery.

5 Conclusion

This study developed a blackout-aware resilient operation framework for V2G-integrated e-DRT under unknown blackout risk. The model evaluates how pre-outage routing, charging, reserve-SOC, and vehicle-positioning decisions shape feasible mobility and emergency-power service once a disruption materializes. By introducing blackout-period grid restrictions, reserve-SOC requirements, and direct modeling of critical-load shortfalls, the framework shifts the evaluation axis from pure operational profit to functional continuity during disruption.

The numerical experiments showed that this shift in evaluation matters, but the mechanism is not a simple profit-for-resilience trade-off. In the representative 14:00–18:00 blackout realization, the resilience-aware policy enters the disruption with a stronger inherited state, raising outage-start fleet SOC from 28.4 to 30.6 kWh. Relative to profit-oriented

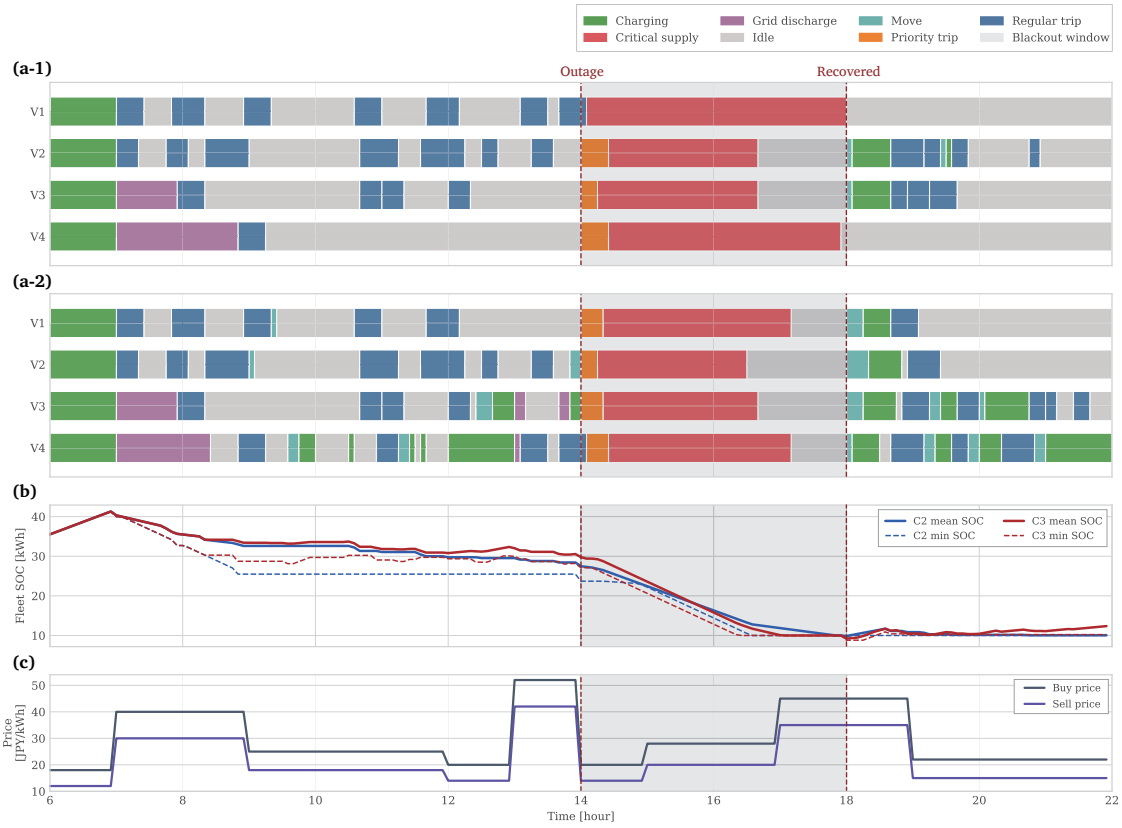


Figure 2: Representative vehicle-activity patterns derived from the computed policies. (a-1) Vehicle schedules for profit-oriented V2G (Case 2). (a-2) Vehicle schedules for resilience-aware V2G (Case 3). Colors indicate vehicle activities, with the main ones being charging (green), regular trips (blue), and critical supply (red). The vertical dashed line marks the blackout onset at 14:00. (b) Time series of fleet SOC for each case. (c) Time series of electricity prices over the day. The post-disruption layer reflects the LP-relaxed recourse approximation used to evaluate the realized disruption.

V2G, this improves passenger service from 46.8% to 54.8%, priority-trip fulfillment from 60.0% to 80.0%, and direct critical-load supply from 38.4% to 42.6%. More broadly, the no-V2G blackout case shows that the day-level objective value can remain high even when emergency functionality collapses. Without explicit coordination of reserve energy and vehicle positioning, the arbitrage logic that is attractive in normal operation can still weaken emergency response and delay service recovery after disruption.
Future work should extend the preparedness-response framework to rolling-horizon and online-updating variants and combine it with richer distribution-network constraints and larger fleet instances in order to better represent infrastructure interdependence at urban scale.

Acknowledgements

This research was performed by the commissioned research fund provided by F-REI (JPFR 26-05-07-01).

References

Bongiovanni, C., Kaspi, M., & Geroliminis, N. (2019). The electric autonomous dial-a-ride problem.

Transportation Research Part B: Methodological, *122*, 436–456. doi: 10.1016/j.trb.2019.03.004

He, Q., Liu, W., & Xi, H. (2025). Dynamic electric vehicle fleets management problem for multi-service platforms with integrated ride-hailing, on-time delivery, and vehicle-to-grid services. *Transportation Research Part B: Methodological*, *199*, 103281. doi: 10.1016/j.trb.2025.103281

Iacobucci, R., McLellan, B., & Tezuka, T. (2018). Modeling shared autonomous electric vehicles: Potential for transport and power grid integration. *Energy*, *158*, 148–163. doi: 10.1016/j.energy .2018.06.024

Iacobucci, R., McLellan, B., & Tezuka, T. (2019). Optimization of shared autonomous electric vehicles operations with charge scheduling and vehicle-to-grid. *Transportation Research Part C: Emerging Technologies*, *100*, 34–52. doi: 10.1016/j.trc.2019.01.011

Kempton, W., & Tomić, J. (2005a). Vehicle-to-grid power fundamentals: Calculating capacity and net revenue. *Journal of Power Sources*, *144*(1), 268–279. doi: 10.1016/j.jpowsour.2004.12.025

Kempton, W., & Tomić, J. (2005b). Vehicle-to-grid power implementation: From stabilizing the grid to supporting large-scale renewable energy. *Journal of Power Sources*, *144*(1), 280–294. doi: 10.1016/j.jpowsour.2004.12.022

Li, X., Huang, J., Guan, Y., Li, Y., & Yuan, Y. (2022). Electric demand-responsive transit routing with opportunity charging strategy. *Transportation Research Part D: Transport and Environment*, *110*, 103427. doi: 10.1016/j.trd.2022.103427

Lian, Y., Lucas, F., & Sörensen, K. (2023). The electric on-demand bus routing problem with partial charging and nonlinear function. *Transportation Research Part C: Emerging Technologies*, *157*, 104368. doi: 10.1016/j.trc.2023.104368

Liao, Z., Taiebat, M., & Xu, M. (2021). Shared autonomous electric vehicle fleets with vehicle-to-grid capability: Economic viability and environmental co-benefits. *Applied Energy*, *302*, 117500. doi: 10.1016/j.apenergy.2021.117500

Lu, C., Maciejewski, M., Wu, H., & Nagel, K. (2023). Demand-responsive transport for students in rural areas: A case study in vulkaneifel, germany. *Transportation Research Part A: Policy and Practice*, *178*, 103837. doi: 10.1016/j.tra.2023.103837

Ma, T. (2021). Two-stage battery recharge scheduling and vehicle-charger assignment policy for dynamic electric dial-a-ride services. *PLOS ONE*, *16*(5), e0251582. doi: 10.1371/journal.pone .0251582

Ma, T., & Fang, Y. (2022). Survey of charging management and infrastructure planning for electrified demand-responsive transport systems: Methodologies and recent developments. *European Transport Research Review*, *14*(1), 36. doi: 10.1186/s12544-022-00560-3

U.S. Energy Information Administration. (2025, June). *Amid regional conflict, the strait of hormuz remains critical oil chokepoint.* Today in Energy. Retrieved from `https://www.eia.gov/todayinenergy/detail.php?id=65504` (Published June 16, 2025; accessed March 28, 2026)

Vansteenwegen, P., Melis, L., Aktaş, D., Galarza Montenegro, B. D., Vieira, F. S., & Sörensen, K. (2022). A survey on demand-responsive public bus systems. *Transportation Research Part C: Emerging Technologies*, *137*, 103573. doi: 10.1016/j.trc.2022.103573

Zeng, T., Moura, S., & Zhou, Z. (2023). Joint mobility and vehicle-to-grid coordination in rebalancing shared mobility-on-demand systems. *IFAC-PapersOnLine*, *56*(2), 6642–6647. doi: 10.1016/j.ifacol.2023.10.365